Supplement of

Dominant Influence of Biomass Combustion and Cross-Border Transport on Nitrogen-Containing Organic Compound Levels in the Southeastern Tibetan Plateau

Meng Wang[1, 2], Qiyuan Wang[1, 3, *], Steven Sai Hang Ho[4], Jie Tian[1], Yong Zhang[1], Shun-cheng Lee[5, *], Junji Cao[6, *]

[1]State Key Laboratory of Loess and Quaternary Geology, Institute of Earth Environment, Chinese Academy of Sciences, Xi'an 710061, China

[2]Department of Civil and Environmental Engineering, The Hong Kong Polytechnic University, Hung Hom, Hong Kong

[3]CAS Center for Excellence in Quaternary Science and Global Change, Xi'an 710061, China

[4]Division of Atmospheric Sciences, Desert Research Institute, Reno, NV89512, United States

[5]Function Hub, Thrust of Earth, Ocean and Atmospheric Sciences, The Hong Kong University of Science and Technology (Guangzhou), 511400 Guangzhou, China

[6]Institute of Atmospheric Physics, Chinese Academy of Sciences, Beijing 100029, China

Correspondence to: Qiyuan Wang (wangqy@ieecas.cn), Shun-cheng Lee (shunchenglee@hkust-gz.edu.cn), and Junji Cao (jjcao@mail.iap.ac.cn)

Text S1. Chemical composition measurements

S1.1 Carbonaceous aerosol fractions

In this study, the determination of organic carbon (OC) and elemental carbon (EC) in the samples was conducted using thermal-optical analysis with a thermal/optical OCEC analyzer. Different protocols, including IMPROVE, NIOSH, and EUSAAR_2, are used for measuring particulate carbon using thermal techniques. The IMPROVE protocol, which was followed in this study, involves analyzing four OC fractions (OC1, OC2, OC3, OC4) and three EC fractions (EC1, EC2, EC3) at specific temperatures. The protocol also defines additional fractions, such as pyrolyzed carbon (OP) and char-EC, and soot-EC. The MDLs for OC and EC were determined to be 0.41 g cm-2 and 0.03 g cm-2, respectively.

S1.2 Water-soluble ion analysis

The Dionex DX-600 ion chromatograph equipped with an IonPac CS12A column was used to determine the concentrations of K^+. Quality assurance/quality control procedures were implemented using standard reference materials provided by the National Research Center for Certified Reference Materials in China. To extract water-soluble ions from the quartz filters, a portion of each filter was placed in a vial with distilled deionized water. Ultrasonic treatment and mechanical shaking were performed to extract the ions, and the resulting extracts were filtered and stored before analysis. For the analysis of inorganic ions, a portion of the filter punch was extracted using ultrapure water. The concentrations of various ions were determined using the Dionex-600 Ion Chromatograph, and standard solutions and blanks were analyzed for calibration and contamination correction.

S1.3 Levoglucosan and arabitol analysis

The filter samples were extracted by placing them in 15 mL vials with 10 mL of distilled deionized water. The extraction process involved subjecting the vials to ultrasonic treatment in a water bath with mechanical shaking for 15 minutes. This extraction was repeated four times with a 30-minute interval between each repetition. The extracts were then filtered using microporous membranes with a pore size of 0.45 mm to remove insoluble materials. To quantify levoglucosan, a Dionex DX-600 ion chromatograph equipped with a pulsed amperometric detector (PAD) was used in high-performance anion exchange chromatography (HPAEC) mode. The separation of levoglucosan was achieved using a Dionex CarboPac MA1 analytical column coupled with a Dionex CarboPac MA1 guard column. A sodium hydroxide solution (612 mM) was used as the eluent at a flow rate of 0.4 mL/min. Each sample analysis took approximately 1 hour. The method detection limit (MDL) for levoglucosan, determined at a signal-to-noise ratio of 3/1, was found to be 1.3 ng/mL.

S1.4 Elemental analysis

The concentrations of major elements such as Ca and Fe, as well as trace elements including Ti, Mn, Cu, As, Pb, Zn, and Br, on the quartz-fiber filters were determined using an ED-XRF analyzer (Epsilon-5 energy-dispersive X-ray fluorescence spectrometry). The instrument employed a three-dimensional polarizing geometry and achieved low detection limits. Quality assurance/quality control procedures were implemented, including replicated analysis of a minimum of 10% of the samples, with repeatability found to be less than 10% for all

analyzed species. The quantification of elements was performed using energy dispersive X-ray fluorescence (ED-XRF) spectrometry with the Epsilon 5 ED-XRF instrument. The instrument utilized a side window X-ray tube with a gadolinium anode and a germanium detector. Each sample was analyzed for approximately 30 minutes to obtain X-ray counts versus photon energies, and the peak energies and areas were used to determine the elemental concentrations.

S1.5 PAHs analysis

The filter punch, measuring 0.53 cm2, was obtained using a stainless steel punch. Two internal standards, n-C24D50 and fluoranthene-d10, were spiked onto the filter punch using dichloromethane. After airdrying, the punch was divided into four portions and loaded into a Pyrex glass TD tube, which was cleaned and prepared beforehand. Glass wool plugs were used to secure the filter pieces in the middle of the tube. The loaded TD tube was placed in the injector port, and desorption took place at increasing temperatures. Simultaneously, the GC oven temperature increased according to a programmed rate. The analysis time for each sample was determined through testing temperature programs, and a new TD tube was used for each analysis to prevent contamination carry-over. Standard calibration curves were established using spiked filters for individual compounds. The GC column used was HP-5MS, and ultrahigh-purity helium was the carrier gas. The mass spectrometric detector (MSD) operated at specific conditions, and the mass scan range covered a specific range. Replicate analyses and backup filters were used to check for contamination, which was found to contribute less than 5%. Ambient samples spiked with standards were analyzed to identify potential interferences. All reported data were corrected for blank values.

S1.6 Receptor model: ME-2 solver

The PMF is a multivariate statistical model to describe the variability of a data matrix, which has been used widely in $PM_{2.5}$ source apportionment studies to analyze the contributions of different sources (Watson et al., 2008; Cao et al., 2013; Zhao et al., 2019). The PMF model can be defined as

$$X = GF + E \qquad (3)$$

where X is the matrix of the measured concentration, G is the contributing matrix, F is the source matrices, and E is the matrix residuals of the model (Paatero and Tapper, 1994). All the elements in PMF model are nonnegative, and the entries in G and F are fitted using a least-squares algorithm. The solution that iteratively minimizes the objective function Q defined as

$$Q = \sum_i \sum_j \left(\frac{e_{ij}}{u_{ij}}\right)^2 \qquad (4)$$

where e_{ij} are the elements of the matrices E and u_{ij} are the errors/uncertainties of measured species which were calculated based on the following equation (Gianini et al., 2012)

$$u_{ij} = \sqrt{(DL_j)^2 + (CV_j\, x_{ij})^2} \qquad (5)$$

where DL_j is the detection limit for compound j, CV_j is the coefficient of the variation for compound j. Paatero (1999) further developed a ME-2 based on the PMF algorithm, which can utilize the constraints provided by the user to enhance the control of rotation for an environmentally meaningful solution (Reyes-Villegas et al., 2016; Bozzetti et al., 2017).

In this study, the ME-2 analysis was performed using the source finder tool SoFi v6.7 (Canonaco et al., 2013) within the Igor Pro software package (Wavemetrics Inc., Lake Oswego, Oregon, USA). The analysis involved aligning daily measurements of 7 nitrogen organic classes with concurrent measurements of 3 carbonaceous materials (EC, POC, and SOC), one water-soluble inorganic ion (K^+), and 10 elements (Ca, Ti, V, Mn, Fe, Cu, As, Br, Pb, and Zn) in the $PM_{2.5}$ fraction. The characteristics of the input species and the correlation matrix of each species can be found in Table S2 and Fig. S3, respectively, providing statistical information for the analysis.

To determine the optimal number of source factors, a series of tests were conducted, ranging from 2 to 12 factors, in free PMF runs. Each factor was initialized from 20 different random starting points. Based on the results, the seven-factor solution obtained from the PMF base run was identified as the optimal solution. This conclusion was supported by a Q/Qexpected value of 1.45 (Fig. S4) and the observation that the scaled residuals were distributed symmetrically between -4 and +4 (Fig. S5). Furthermore, the input total mass of the 24 species and the model-reconstructed total mass of all the factors exhibited a high correlation ($R^2 = 0.99$, slope = 1.03) (Fig. S6), indicating a good agreement between the measured and reconstructed masses. In contrast, the six-factor solution lacked representation of distinct coal combustion sources or traffic emission sources, as these factors were found to be mixed with other fossil fuel emissions. Additionally, solutions with more than seven factors resulted in some factors that had blank values for all carbonaceous species, rendering them meaningless. Consequently, the seven identified sources obtained from the free PMF analysis were biomass burning, coal combustion, industry-related sources, crustal sources, traffic emissions, agriculture activities, and secondary sources. The source attribution based on markers for each factor was consistent with the results obtained from the ME-2 analysis detailed in Section 3.4. However, in some cases, certain factors appeared to be mixed in Fig. S7, where specific source markers were not properly distributed among the expected factors. For example, a significant proportion of SOC was observed in several primary emission sources such as biomass burning (21.5%), industry-related sources (10.9%), and agriculture activities (19.5%). The secondary sources factor in PMF included certain species originating from primary particulates, such as Fe, Ca, and POC. The traffic emissions factor explained a substantial portion (54.2%) of the levoglucosan mass concentration, a specific marker for biomass burning, while 43.1% of the vanadium (V) mass concentration was attributed to the crustal sources factor. This mixing of species among factors may be attributed to the relatively limited number of samples used in the free PMF analysis (64 samples in this study), which could reduce the resolving power of PMF as discussed in (Salameh et al., 2018).

In order to improve the factor separation, a constrained PMF analysis using the "a value" approach of the ME-2 solver was applied (Canonaco et al., 2013). Using the same species concentration matrix and uncertainties matrix, we ran the ME-2 model by SoFi for 7-factor with the constrained matrix as shown in Table S2. The constrained run was performed by adding constraints in the base run resolved factor profiles, so that the tracers are only present in the corresponding sources (Wang et al., 2019). Briefly, the contributions of some species have been fully constrained (set a value to 0) in the factor profiles, as follows:

   (a) Contributions of levoglucosan, a specific marker of biomass burning emissions (Simoneit, 1999), were set to zero in all profiles, except the biomass burning factor;
   (b) Contributions of SOC were set to zero in all profiles, except the secondary sources factor;
   (c) Contributions of vanadium, a typical marker of heavy oil combustion (Viana et al., 2009), were set to zero in all profiles, except the traffic emissions factor;
   (d) Contributions of arsenic (As), markers of coal combustion (Hsu et al., 2016), were only authorized in factors related to coal combustion, imposing their contributions to zero in all other factors;

(e) Contributions of titanium (Ti), a characteristic marker of crustal elements (Zhao et al., 2013), were set to zero in all profiles, except the crustal sources factor;

(f) Contributions of cyclic NOCs (including caprolactam, N,N-diethyl-m-toluamide (DEET), isoindole-1,3-dione, N-butyl-benzen-sulfonamide (NBBS) and benzothiazolone), all of them are synthetic products from the chemical industry (Cheng et al., 2006), were set to zero in all profiles, except the industry-related sources factor.

With these constraints performed in the initial PMF results, the rescaled residual from the constrained PMF analysis were within the range of ±4, except Zn (Fig. S8). Further, good correlations were observed between the measured and calculated concentrations for input species (R^2 = 0.98, slope = 0.92) (Fig. S9), indicating a convincing source apportionment result.

S1.7 Potential source contribution function (PSCF)

The potential source contribution function (PSCF) has been widely used to estimate the transporting areas of air pollutants over long distances, based on air mass back trajectory analysis (Nicolás et al., 2011). The study region can be divided into many equal grid cells (ij), the value of PSCF was calculated as follows:

$$\text{PSCF}_{ij} = \frac{m_{ij}}{n_{ij}} \qquad (6)$$

where i and j is the latitude and longitude. n_{ij} represents the number of endpoints fell in the ij cell, and m_{ij} is on behalf of the number of endpoints in the same cell that are related with samples that are more than the criterion-value (Wang et al., 2015; Liu et al., 2017). The ratio of the counts of selected events (m_{ij}) to the counts of all events (n_{ij}) are often related to sparse trajectory coverage of the more distant grid cells when $m_{ij} \leq n_{ij}$, this may result in PSCF_{ij} with high uncertainty in the apparent high value. But when the value of n is large enough, there is more statistical stability in the calculated value (Polissar et al., 1999). The weighting function W_{ij} should be multiplied into PSCF value for reducing the uncertainty in cells which is less than about 3 times the average value of the end points per each cell (Polissar et al., 2001). The weight function can be described as follows:

$$W_{ij} = \begin{cases} 1 & 80 < N_{ij} \\ 0.7 & 20 < N_{ij} \leq 80 \\ 0.42 & 10 < N_{ij} \leq 20 \\ 0.05 & N_{ij} \leq 10 \end{cases} \qquad (7)$$

In this study, PSCF was used to identify the likely pollution regions that influenced PMF factors loading based on back trajectories. For each trajectory, it includes a range of latitude–longitude coordinates every 1 h backward in a whole day. PSCF was performed on the Zefir (Petit et al., 2017)

Table S1 Data statistics of the 24 chemical species included in PMF analysis (ng m^{-3}).

Species	Arithmetic mean	Median	Minimum	Maximum	BDL[a] (%)	S/N [b]
EC	678.52	618.73	97.30	1909.55	-	4.52
POC	2968.96	2707.33	425.72	8355.48	-	9.07
SOC	953.12	790.20	-	2910.26	-	3.73
K$^+$	107.91	86.22	2.21	373.56	7.81	4.62
Ca	761.25	693.19	33.00	1830.11	-	9.55
Ti	35.85	28.94	1.17	102.91	-	11.83
V	0.90	0.78	0.38	1.75	1.57	5.64
Mn	9.21	8.48	1.93	21.52	1.57	10.15
Fe	357.80	322.00	32.53	938.15	-	9.68
Cu	28.14	25.85	6.89	73.24	-	7.05
As	3.85	2.64	0.38	15.66	-	1.51
Br	4.70	4.66	0.78	11.86	-	2.89
Pb	5.78	5.48	1.34	12.63	1.57	7.94
Zn	46.76	51.02	0.78	88.25	1.57	3.90
Arabitol	4.89	5.04	1.11	11.32	4.69	6.35
Levoglucosan	56.62	46.20	2.54	224.70	-	6.67
PAHs-5rings[c]	0.29	0.23	0.01	1.26	-	1.81
Free amino acids	1092.86	1038.28	370.25	2033.20	-	10.48
Amines	563.30	525.98	190.21	1113.48	-	10.87
Alkyl amides	45.10	41.35	14.90	84.60	-	8.04
Alkyl nitriles	4.69	4.53	1.81	8.18	-	4.43
Urea	266.41	253.73	79.45	588.76	-	9.50
Isocyanates	10.89	10.09	3.34	23.17	-	5.28
Cyclic NOCs	136.16	125.08	42.13	291.93	-	10.73

[a] Below Detection Limit.

[b] S/N=signal to noise ratio.

[c] PAHs-5rings: benzo[b]fluoranthene, benzo[k]fluoranthene, and benzo[a]pyrene.

Table S2 The matrix chemical species constrained in the PMF analysis for the solution of seven factors.

	Biomass burning	Coal combustion	Industry-related	Crustal sources	Traffic emissions	Agriculture activities	Secondary sources
EC	-	-	-	-	-	-	0
POC	-	-	-	-	-	-	0
SOC	0	0	0	0	0	0	-
K$^+$	-	0	0	0	0	-	0
Ca	-	-	-	-	-	-	0
Ti	0	0	0	-	0	0	0
V	0	0	0	0	-	0	0
Mn	0	-	-	-	-	-	0
Fe	0	-	-	-	-	-	0
Cu	0	-	-	0	-	-	0
As	0	-	0	0	0	0	0
Br	0	0	0	0	-	0	0
Pb	0	-	-	0	-	0	0
Zn	-	-	0	-	-	0	0
Arabitol	-	0	0	-	0	0	0
Levoglucosan	-	0	0	0	0	0	0
PAHs-5rings[c]	0	0	0	0	-	0	0
Free amino acids	-	-	-	-	-	-	-
Amines	-	-	-	-	-	-	-
Alkyl amides	-	-	-	-	-	-	-
Alkyl nitriles	-	-	-	-	-	-	-
Urea	-	-	-	-	-	-	-
Isocyanates	-	0	-	0	0	0	0
Cyclic NOCs	0	0	-	0	0	0	0

Notes: The zero values denote species with constraints, and dashes indicate unconstrained elements.

Table S3 Concentrations of individual NOCs in Gaomeigu (ng m^{-3}).

Species	Mean	Standard deviation	Min	Max
Free Amino Acids				
Protein type FAAs				
aspartic acid (Asp)	12.3	21.9	3.55	23.7
serine (Ser)	12.9	7.72	9.59	43.7
glutamic acid (Glu)	7.05	3.00	2.66	17.0
glycine (Gly)	307.3	115.6	130.9	581.0
histidine (His)	8.76	3.59	2.67	16.0
threonine (Thr)	2.34	0.83	0.98	4.80
alanine (Ala)	91.2	36.1	37.9	207.0
proline (Pro)	35.8	13.9	15.1	71.6
cysteine (Cys)	175.6	88.6	32.9	417.0
tyrosine (Tyr)	18.2	8.2	5.9	41.3
valine (Val)	129.2	69.5	25.5	282.1
methionine (Met)	7.39	4.33	1.01	16.8
lysine (Lys)	80.9	45.1	10.2	194.3
isoleucine (Ile)	27.4	12.9	6.41	53.3
leucine (Leu)	31.2	15.2	8.35	65.0
phenylalanine (Phe)	33.0	13.7	14.2	77.1
Non-protein type FAAs				
β-alanine (β-Ala)	79.7	31.9	26.3	165.6
γ-aminobutyric acid (γ-Aba)	12.0	5.57	3.50	24.1
ornithine (Orn)	11.6	6.08	2.04	25.6
Amines				
Aliphatic Amines				
methylamine (MA)	350.3	146.0	121.3	700.8
ethylamine (EA)	154.7	81.4	31.6	348.9
dimethylamine (DMA)	0.69	0.26	0.28	1.38
trimethylamine (TMA)	0.31	0.13	0.10	0.61
diethylamine (DEA)	0.26	0.12	0.07	0.69
triethylamine (TEA)	0.54	0.25	0.17	1.11
N-proplyamine (PA)	0.16	0.07	0.17	0.38
dipropylamine (DPA)	0.04	0.02	0.01	0.07
tripropylamine (TPA)	0.10	0.04	0.03	0.21
N-butylamine (BA)	1.47	0.61	0.55	3.04
iso-butylamine (iso-BA)	0.08	0.04	0.02	0.18
sec-butylamine (sec-BA)	0.20	0.09	0.05	0.56

ethylenediamine (EDA)	0.11	.05	0.03	0.23

Aromatic Amines

phenylamine	0.11	0.05	0.03	0.25
P-aminophenol	0.39	0.17	0.10	0.83
4-ethylphenylamine	0.19	0.07	0.09	0.34
N-methylphenylamine	0.41	0.14	0.18	0.74
iso-propylphenylamine	0.46	0.19	0.17	0.99
2-methylphenylamine	0.09	0.03	0.03	0.17
4-methylphenylamine	0.17	0.08	0.04	0.48
3-propylphenylamine	0.75	0.36	0.25	2.13

Other Amines

ethanolamine	26.5	9.43	11.4	62.1
galactosamine	24.9	11.9	5.64	54.6
2-amino-1-butanol	0.09	0.04	0.03	0.18
N-methylformamide	0.34	0.13	0.12	0.71

Urea	266.4	119.0	79.4	588.8

Alkyl Amides

hexanamide (C6)	5.62	2.26	1.95	12.5
heptanamide (C7)	3.92	2.12	0.81	10.3
octanamide (C8)	2.50	1.02	0.82	5.20
nonanamide (C9)	1.11	0.47	0.39	2.32
decanamide (C10)	1.56	0.75	0.31	4.38
undecanamide (C11)	1.15	0.43	0.43	2.02
dodecanamide (C12)	1.70	0.77	0.41	3.57
tridecanamide (C13)	1.25	0.56	0.37	3.23
tetradecanamide (C14)	3.00	1.44	0.72	6.49
pentadecanamide (C15)	2.17	1.02	0.69	5.20
hexadecanamide (C16)	2.66	1.21	0.67	5.62
heptadecanamide (C17)	1.79	0.76	0.61	4.29
octadecanamide (C18)	2.36	1.07	0.60	4.90
nonadecanamide (C19)	1.69	0.84	0.52	4.21
icosanamide (C20)	2.01	0.95	0.71	4.69
hexadecenamide (C16:1)	7.57	2.97	3.09	15.5
octadecenamide (C18:1)	3.04	1.33	1.08	6.37

Nitriles

hexanenitrile (C6)	0.15	0.06	0.06	0.35

heptanenitrile (C7)	0.32	0.14	0.11	0.63
octanenitrile (C8)	0.32	0.155	0.07	0.66
nonanenitrile (C9)	0.23	0.09	0.06	0.51
decanenitrile (C10)	0.35	0.13	0.12	0.61
undecanenitrile (C11)	0.29	0.11	0.10	0.58
dodecanenitrile (C12)	0.39	0.16	0.15	0.85
tridecanenitrile (C13)	0.30	0.12	0.11	0.61
tetradecanenitrile (C14)	0.45	0.19	0.12	1.04
pentadecanenitrile (C15)	0.22	0.08	0.08	0.45
hexadecanenitrile (C16)	0.49	0.19	0.18	1.20
heptadecanenitrile (C17)	0.37	0.15	0.12	0.79
octadecanenitrile (C18)	0.39	0.15	0.14	0.73
nonadecanenitrile (C19)	0.21	0.09	0.07	0.40
icosanenitrile (C20)	0.21	0.09	0.08	0.44
Cyclic NOCs				
caprolactam	54.2	23.4	16.1	112.4
N, N-diethyl-m-toluamide (DEET)	5.79	3.23	1.13	14.3
isoindole-1,3-dione	50.7	25.3	12.4	118.0
N-butyl-benzen-sulfonamide (NBBS)	22.1	10.6	6.52	47.5
benzothiazolone	3.36	1.63	1.07	7.35
Isocyanates				
methyl isocyanate	2.01	0.88	0.66	4.16
toluene-2,4-diisocyanate	2.38	1.05	0.63	5.38
toluene-2,6-diisocyanate	0.52	0.28	0.09	1.17
isophorone diisocyanate	0.64	0.32	0.11	1.31
1,6-hexamethylene diisocyanate	0.97	0.44	0.37	2.30
ethyl isocyanate	2.58	1.34	0.62	7.33
phenyl isocyanate	0.84	0.32	1.72	0.40
propyl isocyanate	0.94	0.43	0.25	2.14
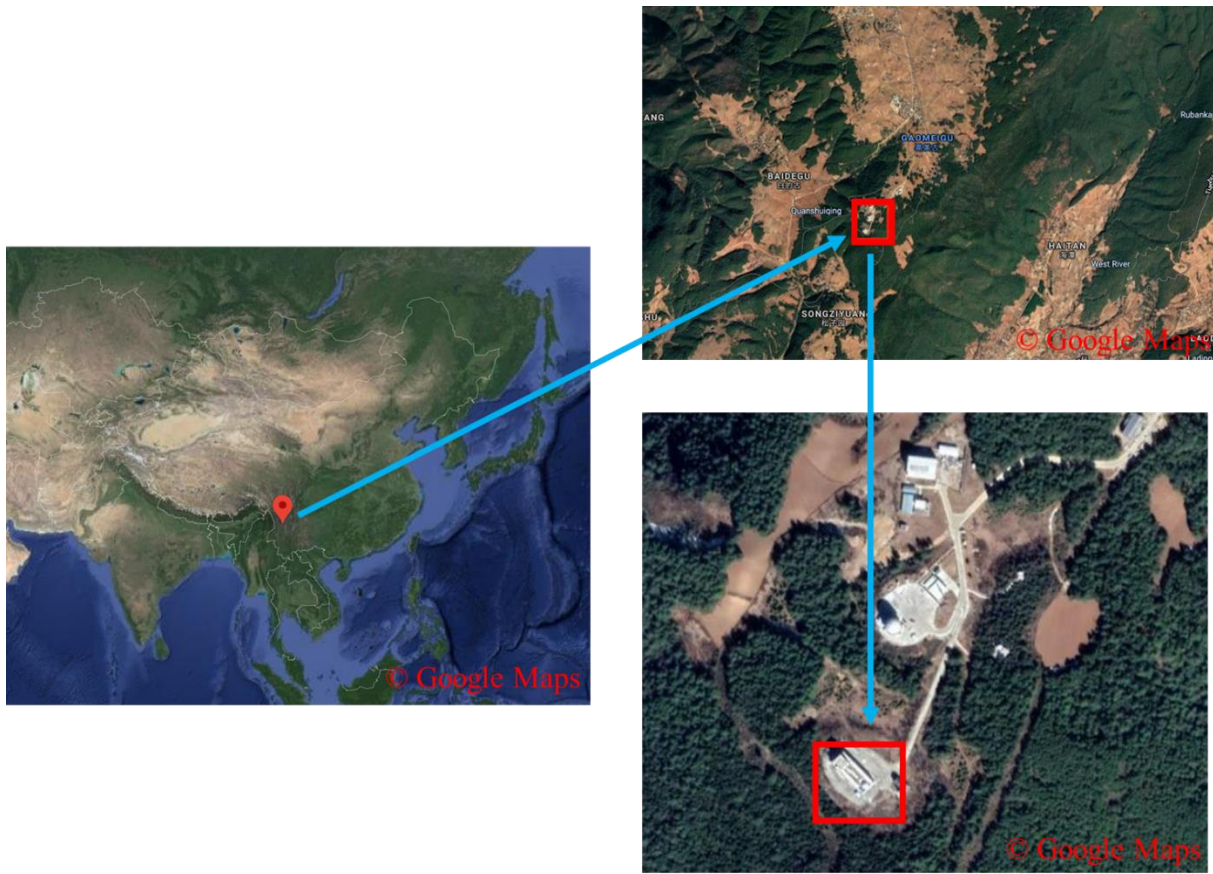
Fig. S1 Map of the sampling location (Gaomeigu, Yunnan, China). The site is marked with the red Google pin.
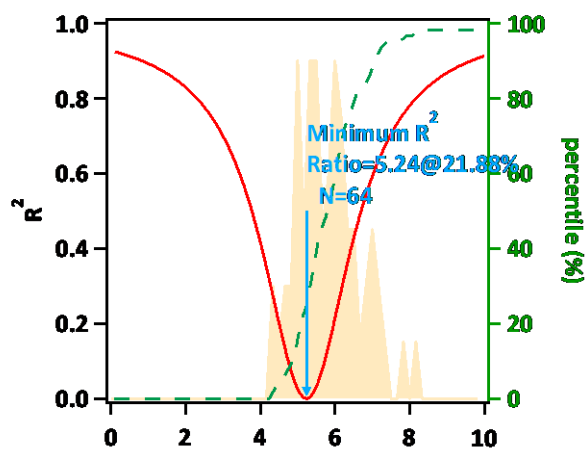
Fig. S2 Illustration of the MRS method to determine (OC/EC)pri using offline data of daily OC and EC measurements in Gaomeigu.
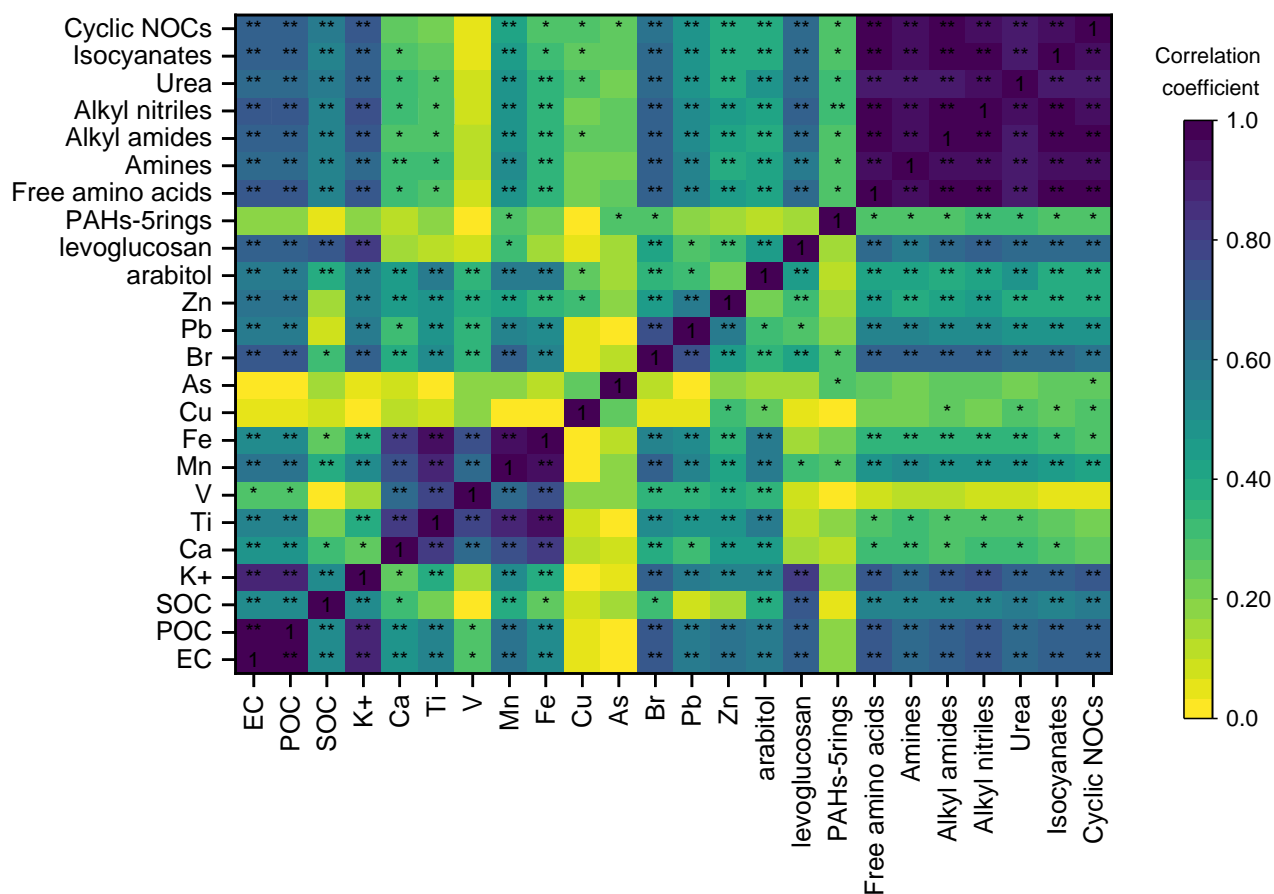
a **. Correlation is significant at the 0.01 level (2-tailed).

Fig. S3 Correlation matrix of the 24 variables.
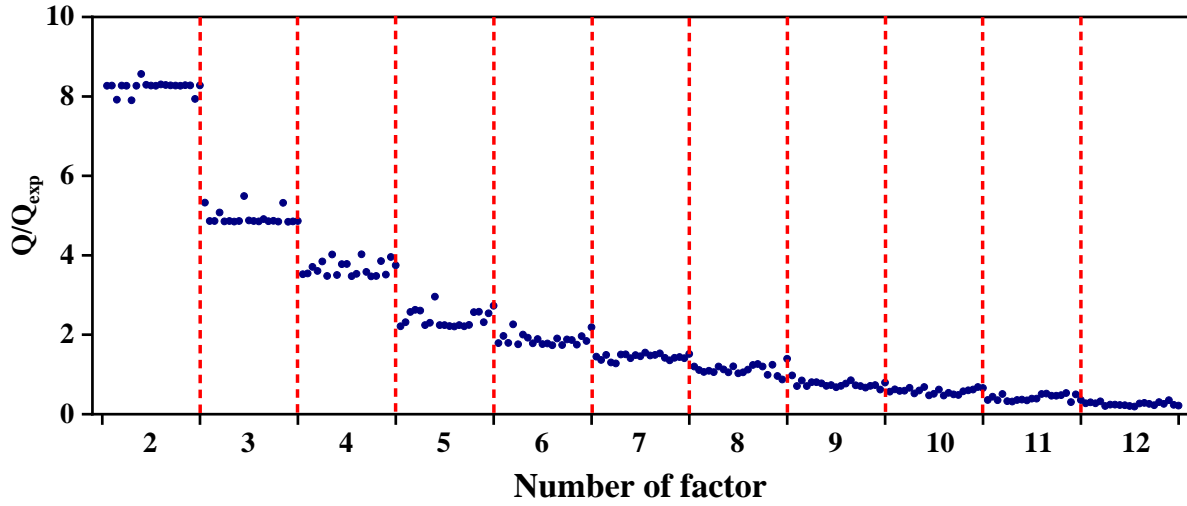
Fig. S4 Variation of the ratio $Q/Q_{expected}$ for p from 2 to 12 factors (seed = 20).
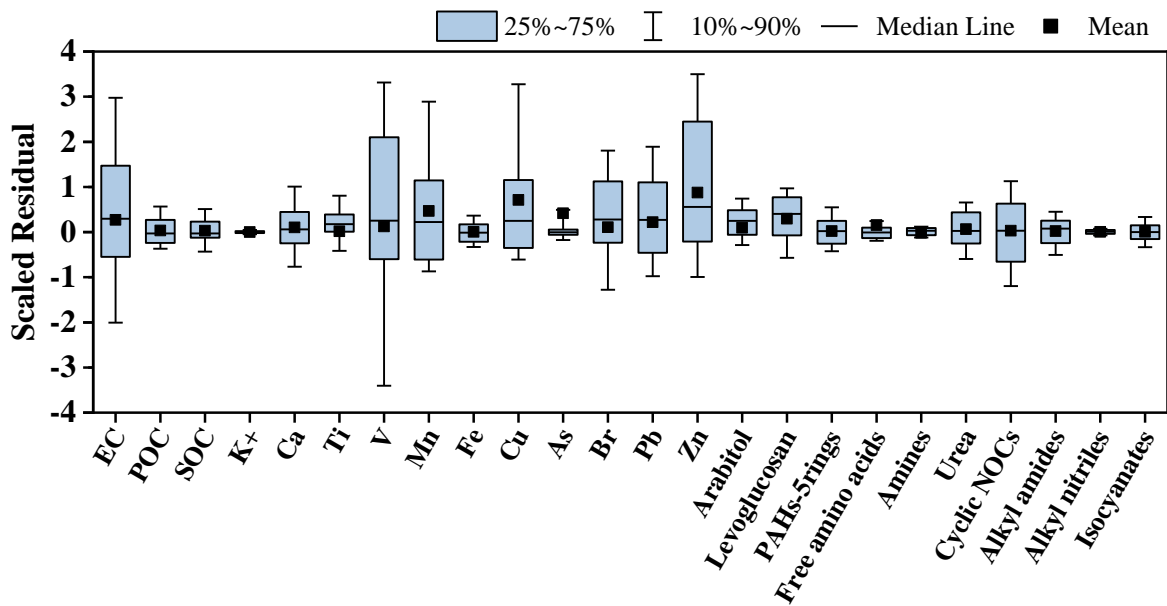
Fig. S5 Distribution of the residuals scaled by the uncertainty for each variable of free PMF.
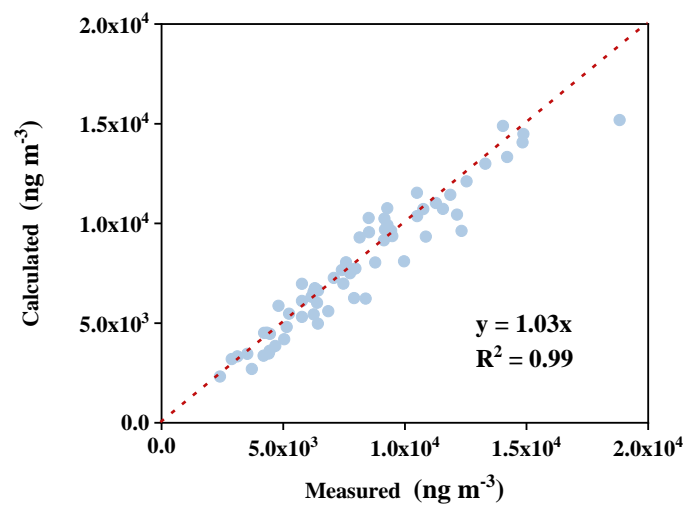
Fig. S6 Regression between calculated and measured concentrations of the target compounds by free PMF.
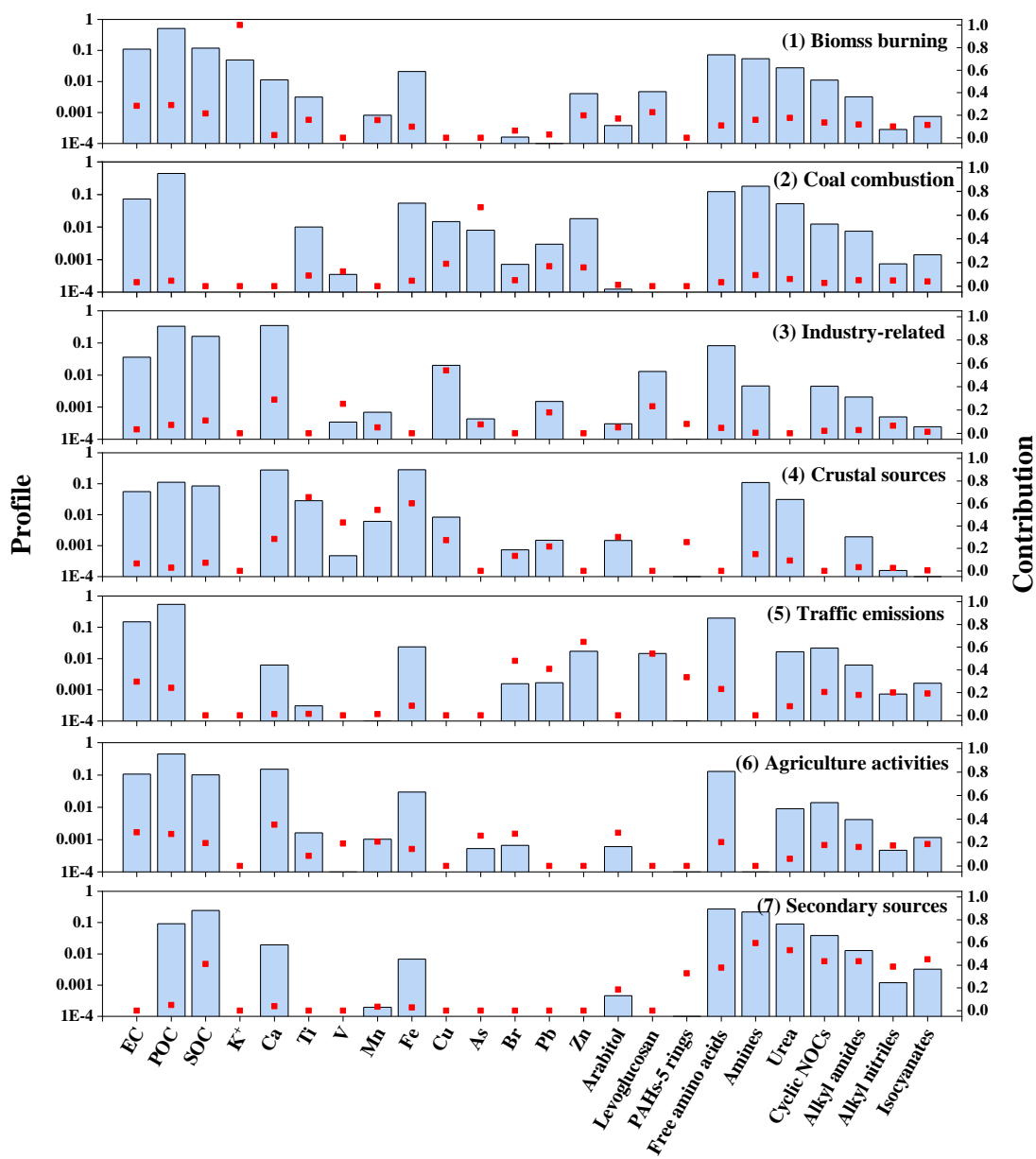
Fig. S7 Factor profiles and contribution (% of species) of seven factors deduced by free PMF.
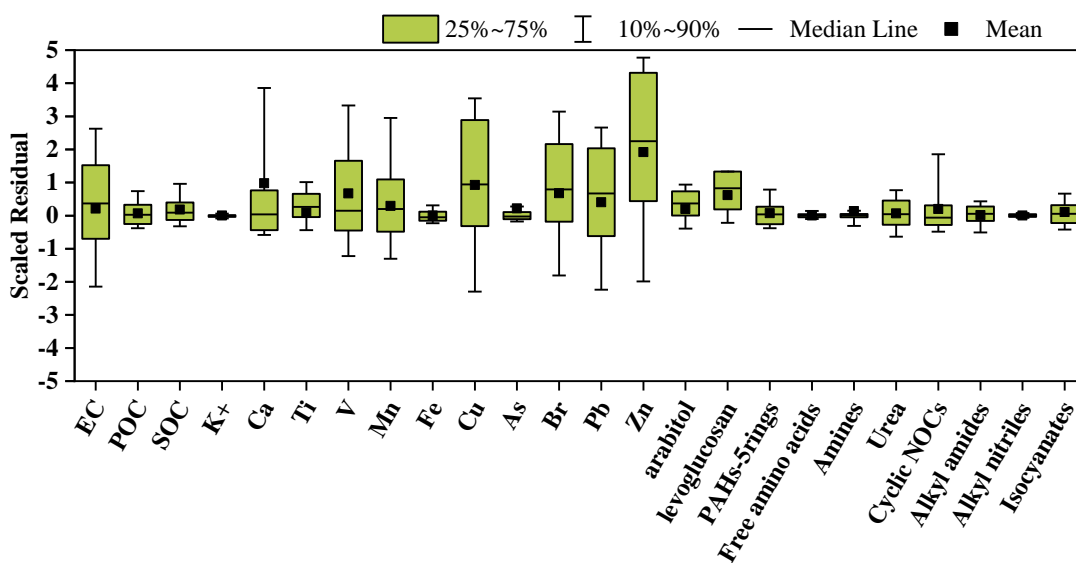
Fig. S8 Distribution of the residuals scaled by the uncertainty for each variable of constrained PMF.
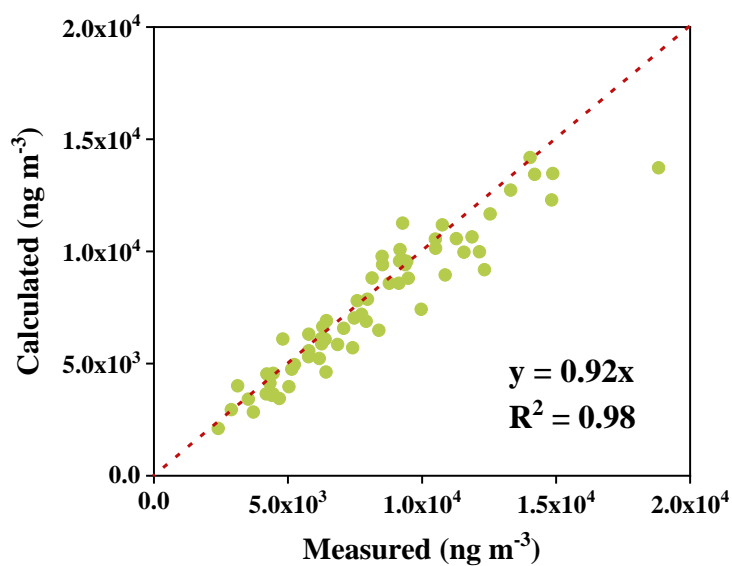
Fig. S9 Regression between calculated and measured concentrations of the target compounds by constrained PMF.
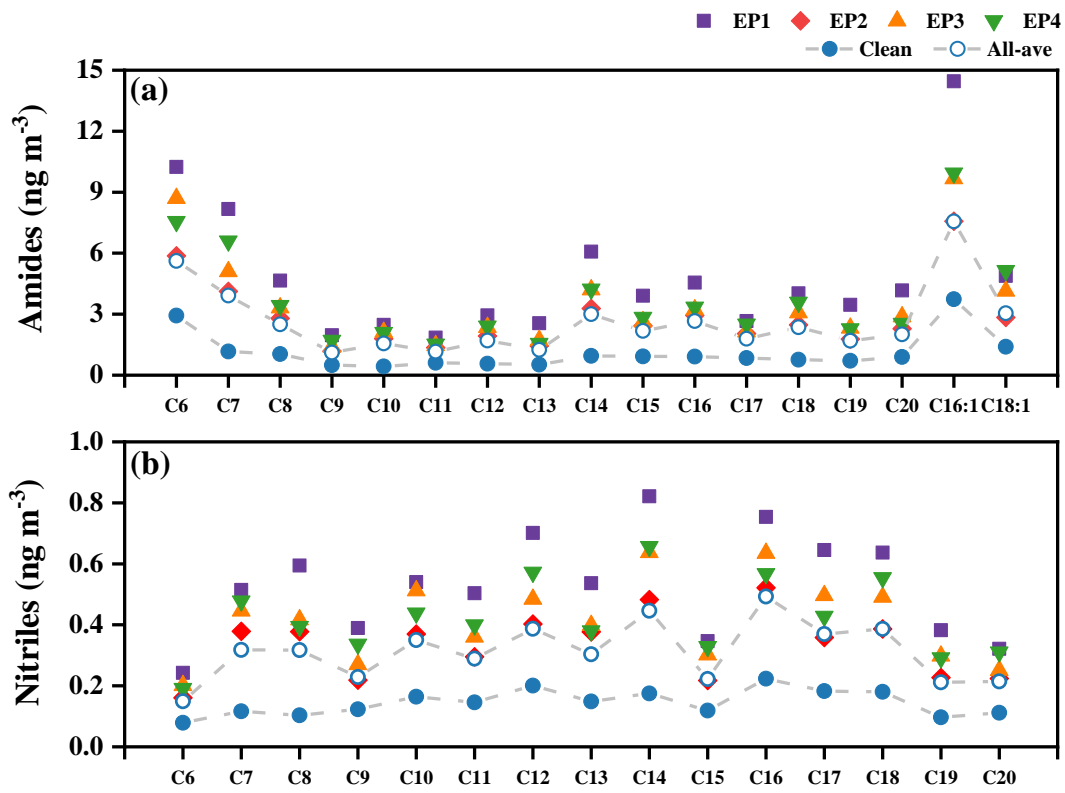
Fig. S10 Concentrations and carbon number distributions of (a) alkyl amides ranging from C6 to C20 and (b) nitriles ranging from C6 to C20 on $PM_{2.5}$ from Gaomeigu.
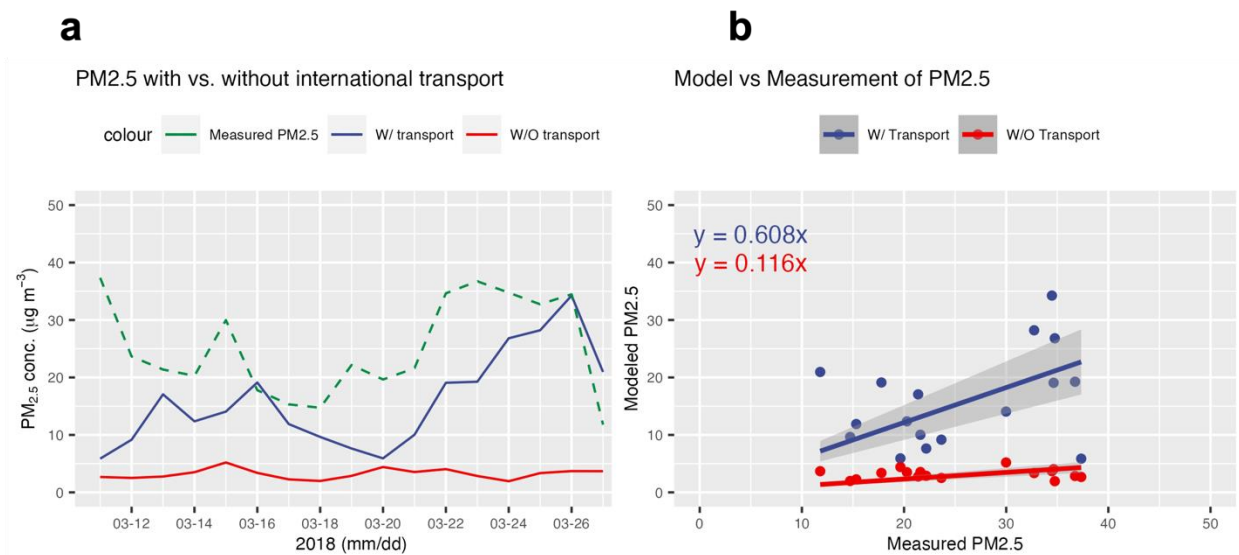
Fig. S11: (a) Time series comparison of measured versus modeled PM2.5 concentrations at the GMG station; (b) Scatter plot correlating the observed with the modeled PM2.5 concentrations, including linear regression lines for the two modeling scenarios, each constrained with a zero intercept.
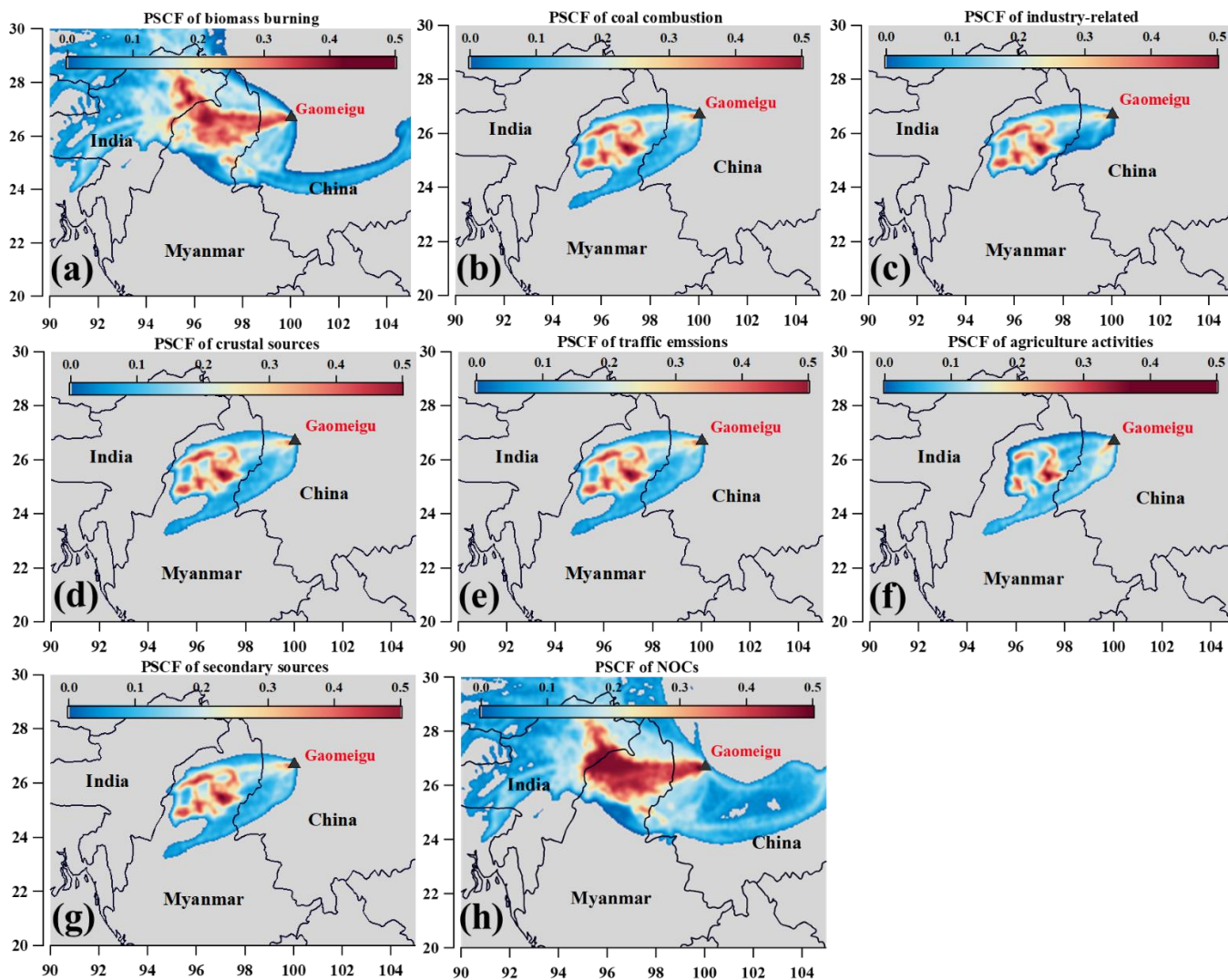
Fig. 12. PSCF results for each identified source in the study, including (a) biomass burning; (b) coal combustion; (c) industry-related sources; (d) crustal sources; (e) traffic emissions; (f) agriculture activities; (g) secondary sources; and (h) total NOCs, color-coded based on the percentage during each period. The PSCF results were plotted using ZeFir. The black triangle represents the sampling site in Gaomeigu.

References:

Bozzetti, C., Sosedova, Y., Xiao, M., Daellenbach, K. R., Ulevicius, V., Dudoitis, V., Mordas, G., Byčenkienė, S., Plauškaitė, K., Vlachou, A., Golly, B., Chazeau, B., Besombes, J. L., Baltensperger, U., Jaffrezo, J. L., Slowik, J. G., El Haddad, I., and Prévôt, A. S. H.: Argon offline-AMS source apportionment of organic aerosol over yearly cycles for an urban, rural, and marine site in northern Europe, Atmos. Chem. Phys., 17, 117-141, 10.5194/acp-17-117-2017, 2017.

Canonaco, F., Crippa, M., Slowik, J. G., Baltensperger, U., and Prévôt, A. S. H.: SoFi, an IGOR-based interface for the efficient use of the generalized multilinear engine (ME-2) for the source apportionment: ME-2 application to aerosol mass spectrometer data, Atmos. Meas. Tech., 6, 3649-3661, doi:10.5194/amt-6-3649-2013, 2013.

Cao, J. J., Zhu, C. S., Tie, X. X., Geng, F. H., Xu, H. M., Ho, S. S. H., Wang, G. H., Han, Y. M., and Ho, K. F.: Characteristics and sources of carbonaceous aerosols from Shanghai, China, Atmos. Chem. Phys., 13, 803-817, 10.5194/acp-13-803-2013, 2013.

Cheng, Y., Li, S.-M., and Leithead, A.: Chemical Characteristics and Origins of Nitrogen-Containing Organic Compounds in PM2.5 Aerosols in the Lower Fraser Valley, Environ. Sci. Technol., 40, 5846-5852, 10.1021/es0603857, 2006.

Gianini, M., Fischer, A., Gehrig, R., Ulrich, A., Wichser, A., Piot, C., Besombes, J.-L., and Hueglin, C.: Comparative source apportionment of PM10 in Switzerland for 2008/2009 and 1998/1999 by Positive Matrix Factorisation, Atmos. Environ., 54, 149-158, 2012.

Hsu, C.-Y., Chiang, H.-C., Lin, S.-L., Chen, M.-J., Lin, T.-Y., and Chen, Y.-C.: Elemental characterization and source apportionment of PM10 and PM2.5 in the western coastal area of central Taiwan, Sci. Total Environ., 541, 1139-1150, https://doi.org/10.1016/j.scitotenv.2015.09.122, 2016.

Liu, B., Wu, J., Zhang, J., Wang, L., Yang, J., Liang, D., Dai, Q., Bi, X., Feng, Y., Zhang, Y., and Zhang, Q.: Characterization and source apportionment of PM2.5 based on error estimation from EPA PMF 5.0 model at a medium city in China, Environ. Pollut., 222, 10-22, https://doi.org/10.1016/j.envpol.2017.01.005, 2017.

Nicolás, J., Chiari, M., Crespo, J., Galindo, N., Lucarelli, F., Nava, S., and Yubero, E.: Assessment of potential source regions of PM2.5 components at a southwestern Mediterranean site, Tellus B: Chemical and Physical Meteorology, 63, 96-106, 10.1111/j.1600-0889.2010.00510.x, 2011.

Paatero, P.: The Multilinear Engine—A Table-Driven, Least Squares Program for Solving Multilinear Problems, Including the n-Way Parallel Factor Analysis Model, Journal of Computational and Graphical Statistics, 8, 854-888, 10.1080/10618600.1999.10474853, 1999.

Paatero, P. and Tapper, U.: Positive matrix factorization: A non-negative factor model with optimal utilization of error estimates of data values, Environmetrics, 5, 111-126, 10.1002/env.3170050203, 1994.

Petit, J. E., Favez, O., Albinet, A., and Canonaco, F.: A user-friendly tool for comprehensive evaluation of the geographical origins of atmospheric pollution: Wind and trajectory analyses, Environ. Modell. Softw., 88, 183-187, 2017.

Polissar, A. V., Hopke, P. K., and Harris, J. M.: Source Regions for Atmospheric Aerosol Measured at Barrow, Alaska, Environ. Sci. Technol., 35, 4214-4226, 10.1021/es0107529, 2001.

Polissar, A. V., Hopke, P. K., Paatero, P., Kaufmann, Y. J., Hall, D. K., Bodhaine, B. A., Dutton, E. G., and Harris, J. M.: The aerosol at Barrow, Alaska: long-term trends and source locations, Atmos. Environ., 33,

2441-2458, https://doi.org/10.1016/S1352-2310(98)00423-3, 1999.

Reyes-Villegas, E., Green, D. C., Priestman, M., Canonaco, F., Coe, H., Prévôt, A. S. H., and Allan, J. D.: Organic aerosol source apportionment in London 2013 with ME-2: exploring the solution space with annual and seasonal analysis, Atmos. Chem. Phys., 16, 15545-15559, 10.5194/acp-16-15545-2016, 2016.

Salameh, D., Pey, J., Bozzetti, C., El Haddad, I., Detournay, A., Sylvestre, A., Canonaco, F., Armengaud, A., Piga, D., Robin, D., Prevot, A. S. H., Jaffrezo, J. L., Wortham, H., and Marchand, N.: Sources of PM2.5 at an urban-industrial Mediterranean city, Marseille (France): Application of the ME-2 solver to inorganic and organic markers, Atmospheric Research, 214, 263-274, https://doi.org/10.1016/j.atmosres.2018.08.005, 2018.

Simoneit, B. R.: A review of biomarker compounds as source indicators and tracers for air pollution, Environmental Science and Pollution Research, 6, 159-169, 1999.

Viana, M., Amato, F., Alastuey, A., Querol, X., Moreno, T., García Dos Santos, S., Herce, M. D., and Fernández-Patier, R.: Chemical Tracers of Particulate Emissions from Commercial Shipping, Environ. Sci. Technol., 43, 7472-7477, 10.1021/es901558t, 2009.

Wang, Q., Huang, X. H. H., Tam, F. C. V., Zhang, X., Liu, K. M., Yeung, C., Feng, Y., Cheng, Y. Y., Wong, Y. K., Ng, W. M., Wu, C., Zhang, Q., Zhang, T., Lau, N. T., Yuan, Z., Lau, A. K. H., and Yu, J. Z.: Source apportionment of fine particulate matter in Macao, China with and without organic tracers: A comparative study using positive matrix factorization, Atmos. Environ., 198, 183-193, https://doi.org/10.1016/j.atmosenv.2018.10.057, 2019.

Wang, Q. Y., Huang, R. J., Cao, J. J., Tie, X. X., Ni, H. Y., Zhou, Y. Q., Han, Y. M., Hu, T. F., Zhu, C. S., Feng, T., Li, N., and Li, J. D.: Black carbon aerosol in winter northeastern Qinghai-Tibetan Plateau, China: The source, mixing state and optical property, Atmos. Chem. Phys., 15, 13059-13069, 10.5194/acp-15-13059-2015, 2015.

Watson, J. G., Antony Chen, L. W., Chow, J. C., Doraiswamy, P., and Lowenthal, D. H.: Source Apportionment: Findings from the U.S. Supersites Program, Journal of the Air & Waste Management Association, 58, 265-288, 10.3155/1047-3289.58.2.265, 2008.

Zhao, Z., Wang, Q., Li, L., Han, Y., Ye, Z., Pongpiachan, S., Zhang, Y., Liu, S., Tian, R., and Cao, J.: Characteristics of PM2.5 at a High-Altitude Remote Site in the Southeastern Margin of the Tibetan Plateau in Premonsoon Season, Atmosphere, 10, 645, 2019.

Zhao, Z., Cao, J., Shen, Z., Xu, B., Zhu, C., Chen, L.-W. A., Su, X., Liu, S., Han, Y., Wang, G., and Ho, K.: Aerosol particles at a high-altitude site on the Southeast Tibetan Plateau, China: Implications for pollution transport from South Asia, J. Geophys. Res. Atmos., 118, 11,360-311,375, https://doi.org/10.1002/jgrd.50599, 2013.